

RESIDUAL PRINT IN ELASTIC-PLASTIC CONTACTS

Ioan UNGUREANU, Sergiu SPINU

University "Stefan cel Mare" of Suceava, ROMANIA
e-mail: ionut@fim.usv.ro, sergiu.spinu@fim.usv.ro

Keywords: residual print, elastic-plastic contact, fast Fourier transform, experimental simulation

Abstract: Residual print in elastic-plastic contacts accounts for plastic strain region contribution to surface normal displacement, thus modifying pressure distribution by superimposing the elastic part of displacements. The mathematical formulation is based on Betti's reciprocal theorem, and involves convolution-type products, which are computed using spectral methods. When contacting bodies receive the same elastic-plastic properties and contact geometry, interference equation is updated by modifying the term related to residual displacement. Residual print depths obtained experimentally from indentation of a lead specimen with a rigid sphere match well the numerical predictions of the newly proposed computer code.

1. INTRODUCTION

Assessment of residual print is primordial to the solution of elastic-plastic contact problem, as residual displacement, namely the displacement induced by the plastic strain region, superimpose the elastic displacement, namely the displacement induced by contact pressure. The resulting interference equation can be used in a purely elastic contact solver to assess pressure distribution and contact area in the elastic-plastic contact. With residual part of displacement computed, elastic-plastic contact can be treated as an elastic contact with a modified initial contact geometry. This formulation, currently used in most elastic-plastic contact solvers, [7,11,15], is based on the Betti's reciprocal theorem.

Although Mayeur, [10], developed the first algorithm for elastic-plastic contact modeling, his implementation was restricted to the two-dimensional case. Computation of residual displacement in the three-dimensional elastic-plastic contact was advanced by Jacq [6]. Alternative formulas for influence coefficients were derived by Antaluca, [1], who added the influence of tangential loading in elastic-plastic contacts. Both formulations are based on the reciprocal theorem, and take advantage of the deviatoric character of plastic strain (namely, the first invariant of plastic strain tensor is nil).

An alternative strategy for residual displacement computation was suggested by Liu and Wang, [9], and involves derivatives of four key integrals, resulting in increased model complexity.

The algorithm used in this paper is similar to the one originally proposed by Jacq, [6]. The Discrete Convolution Fast Fourier Transform algorithm, advanced by Liu, Wang and Liu, [8], is used to speed up the computation of two-dimensional convolution products. Residual term in interference equation is modified for the case when both contacting bodies are elastic-plastic, described by the same hardening law. Experimental validation of residual print depth variation with loading level is also provided.

2. NUMERICAL MODELING

Using Betti's reciprocal theorem, Mayeur, [10], expressed the displacements and the stresses in an elastic isotropic half-space in the presence of plastic strains. A complete model for the three-dimensional elastic-plastic contact was later advanced by Jacq. et al. [7]. According to this formulation, if two independent loads are applied to an elastic body of volume Ω and of boundary Γ , generating two independent states (u, ε, σ) and $(u^*, \varepsilon^*, \sigma^*)$, and the latter corresponds to a unit load applied along the direction of \bar{x}_3 , in a point A of the boundary:

$$p_3^*(M) = \begin{cases} 0, & M \neq A; \\ (dx_1 dx_2)^{-1}, & M = A. \end{cases} \quad (1)$$

the following equation holds:

$$u_3(A) = \int_{\Gamma_C} u_{33}^*(M, p_3^*(A)) p_3(M) d\Gamma + 2\mu \int_{\Omega_p} \varepsilon_{ij}^p(M) \varepsilon_{3ij}^*(M, p_3^*(A)) d\Omega. \quad (2)$$

Here, Γ_C is the boundary subdomain with normal tractions p_3 , and Ω_p the volume subdomain with existing plastic strains ε^p , both corresponding to state (u, ε, σ) , μ Lamé's constant and M the integration point. This point is located within Γ_C in the first term of eq. (2) and within Ω_p in the second. Consequently, $u_{33}^*(M, p_3^*(A))$ is the displacement in the direction of \bar{x}_3 , and $\varepsilon_{3ij}^*(M, p_3^*(A))$ is the strain tensor induced at point M by the loading described by eq. (1). By varying the position of A on Γ and by applying superposition principle, normal displacement in every point of the boundary can be assessed. The second term in (2), which is expressed as a volume integral, represents the residual part of the displacement, namely the deflection that would persist after unloading elastically the considered body:

$$u_3^r(A) = 2\mu \int_{\Omega_p} \varepsilon_{ij}^p(M) \varepsilon_{3ij}^*(M, A) d\Omega. \quad (3)$$

As the region of plastic strains Ω_p can be arbitrarily shaped, this integral can only be computed numerically. The numerical formulation is based on dividing the region of plastic strains Ω_p in a set of N cuboids of elementary volume Ω_c having uniform plastic strains in each elementary cuboid. Consequently, the continuous distribution of ε^p in Ω_p is assumed as piece-wise constant and Ω_p is substituted by a reunion of elementary cuboids Ω_{pn} . With this formulation, the residual displacement can be expressed as the sum of contributions of all elementary cuboids:

$$u_3^r(A) = 2\mu \sum_{k=1}^N \varepsilon_{ij}^p(k) \int_{\Omega_c} \varepsilon_{3ij}^*(k, A), \quad (4)$$

or, by indexing the cuboids with a set of three integers and by denoting the cuboid sides with Δ_1, Δ_2 and Δ_3 :

$$u_3^r(i, j, 0) = 2\mu \sum_{(\ell, m, n) \in \Omega_{pn}} \left(\varepsilon_{\zeta\zeta}^p(\ell, m, n) \cdot \int_{x_3(n)-\Delta_3/2}^{x_3(n)+\Delta_3/2} \int_{x_2(m)-\Delta_2/2}^{x_2(m)+\Delta_2/2} \int_{x_1(\ell)-\Delta_1/2}^{x_1(\ell)+\Delta_1/2} \varepsilon_{3\zeta\zeta}^*(\ell - x_1(i), m - x_2(j), n) dx_1 dx_2 dx_3 \right), \quad (5)$$

The tensor ε_3^* , representing strains due to a unit concentrated force applied on surface boundary, are known from Boussinesq fundamental solutions, [4], which represent, in terms of spectral methods, the corresponding Green functions. In order to compute the

influence coefficients, functions d_{ij} are defined as primitives of functions $2\mu\varepsilon_{3ij}^* = \mu(u_{3i,i}^* + u_{3i,i}^*)$ with respect to directions of \bar{x}_1, \bar{x}_2 and of \bar{x}_3 , and functions $d_{ij}, i < j$, as primitives of $2\mu(\varepsilon_{3ij}^* + \varepsilon_{3ji}^*) = 2\mu(u_{3i,j}^* + u_{3j,i}^*)$ with respect to the same directions. The influence coefficients can then be computed according to the following relation:

$$D_{\zeta\xi}(i, j, k) = \begin{pmatrix} d_{\zeta\xi}(x_1(i) + \frac{\Delta_1}{2}, x_2(j) + \frac{\Delta_2}{2}, x_3(k) + \frac{\Delta_3}{2}) + d_{\zeta\xi}(x_1(i) + \frac{\Delta_1}{2}, x_2(j) - \frac{\Delta_2}{2}, x_3(k) - \frac{\Delta_3}{2}) + \\ d_{\zeta\xi}(x_1(i) - \frac{\Delta_1}{2}, x_2(j) + \frac{\Delta_2}{2}, x_3(k) - \frac{\Delta_3}{2}) + d_{\zeta\xi}(x_1(i) - \frac{\Delta_1}{2}, x_2(j) - \frac{\Delta_2}{2}, x_3(k) + \frac{\Delta_3}{2}) - \\ d_{\zeta\xi}(x_1(i) + \frac{\Delta_1}{2}, x_2(j) + \frac{\Delta_2}{2}, x_3(k) - \frac{\Delta_3}{2}) - d_{\zeta\xi}(x_1(i) + \frac{\Delta_1}{2}, x_2(j) - \frac{\Delta_2}{2}, x_3(k) + \frac{\Delta_3}{2}) - \\ d_{\zeta\xi}(x_1(i) - \frac{\Delta_1}{2}, x_2(j) + \frac{\Delta_2}{2}, x_3(k) + \frac{\Delta_3}{2}) - d_{\zeta\xi}(x_1(i) - \frac{\Delta_1}{2}, x_2(j) - \frac{\Delta_2}{2}, x_3(k) - \frac{\Delta_3}{2}) \end{pmatrix}. \quad (6)$$

The following primitives can be used:

$$d_{11}(x_1, x_2, x_3) = \frac{1}{2\pi} \left((1-2\nu)x_3 \left(\tan^{-1} \left(\frac{x_2 x_3}{x_1 r} \right) - \tan^{-1} \left(\frac{x_2}{x_1} \right) \right) - 2\nu x_1 \ln(x_2 + r) \right); \quad (7)$$

$$d_{33}(x_1, x_2, x_3) = \frac{1}{2\pi} \left(\begin{aligned} &2(1-\nu) \left(x_3 \tan^{-1} \left(\frac{x_1}{x_3} \right) + x_2 \ln(x_1 + r) + x_1 \ln(x_2 + r) \right) + \\ &+(2\nu-1)x_3 \tan^{-1} \left(\frac{x_1 x_2}{x_3 r} \right) \end{aligned} \right); \quad (8)$$

$$d_{12}(x_1, x_2, x_3) = \frac{2}{\pi} (-2\nu r - (1-2\nu)x_3 \ln(x_3 + r)); \quad (9)$$

$$d_{23}(x_1, x_2, x_3) = \frac{1}{\pi} \left(x_1 \tanh^{-1} \left(\frac{r}{x_3} \right) - x_2 \tan^{-1} \left(\frac{x_1 x_3}{x_2 r} \right) \right); \quad (10)$$

$$d_{13}(x_1, x_2, x_3) = d_{23}(x_2, x_1, x_3); \quad d_{22}(x_1, x_2, x_3) = d_{11}(x_2, x_1, x_3). \quad (11)$$

Eq. (5) written with respect to indices of elementary cells takes the following form:

$$u_3^r(i, j, 0) = \sum_{(\ell, m, n) \in \Omega_{pn}} \varepsilon_{\zeta\xi}^p(\ell, m, n) D_{\zeta\xi}(\ell - i, m - j, n), \quad (12)$$

with summation over $\zeta, \xi = 1, 2, 3, \zeta \leq \xi$. If expression $D_{\zeta\xi}(i - \ell, j - m, n)$ is used in relation (12) instead of $D_{\zeta\xi}(\ell - i, m - j, n)$, namely the point of integration and the point of observation are interchanged, eq. (12) takes the following form:

$$u_3^r(i, j, 0) = \sum_{(\ell, m, n) \in \Omega_{pn}} D_{\zeta\xi}(i - \ell, j - m, n) \varepsilon_{\zeta\xi}^p(\ell, m, n), \quad (13)$$

which represents a discrete cyclic convolution with respect to directions \bar{x}_1 and \bar{x}_2 . Efficient computation for this product is available through Discrete Convolution Fast Fourier (DCFFT) technique advanced by Liu, Wang and Liu, [8].

An additional reduction of necessary computational resources is performed if complex influence coefficients $\overline{D_{ij}}$ are defines as:

$$\overline{D_{ij}} = D_{ij} + i \cdot D_{i+1j}, \quad (14)$$

and complex plastic strains:

$$\overline{\varepsilon_{ij}^p} = \varepsilon_{ij}^p - i \cdot \varepsilon_{i+1j}^p. \quad (15)$$

Convolution of terms (14) and (15) yields:

$$\overline{D_{ij}} \otimes \overline{\varepsilon_{ij}^p} = D_{ij} \otimes \varepsilon_{ij}^p + D_{i+1j} \otimes \varepsilon_{i+1j}^p + i \cdot (D_{i+1j} \otimes \varepsilon_{ij}^p - D_{ij} \otimes \varepsilon_{i+1j}^p) \quad (16)$$

which returns, on the real part, the contribution of two members of the tensor, computed in one complex convolution operation only. The complex part of the right member in (16) is discarded. With this approach, the number of fast Fourier transforms (FFT) required to assess contribution of two terms of the plastic strain tensor is reduced considerably: one direct FFT and one inverse FFT (IFFT), instead of three FFTs and two IFFTs.

3. RESIDUAL PRINT IN ELASTIC-PLASTIC CONTACT

The algorithm for computation of residual displacement described in the previous section was implemented in a Matlab program and integrated in an elastic-plastic contact solver. The full process of simulating non-conforming contacts in elastic-plastic domain is presented in [14]. Some results are depicted below.

The circular contact between a rigid sphere of radius $R = 105 \cdot 10^{-6} m$ and an elastic-plastic half-space was loaded incrementally up to $W = 0.650N$, corresponding to an equivalent hertzian pressure of $p_H = 8470 MPa$ and a Hertz contact radius of $a_H = 6.053 \mu m$. The elastic parameters of the half-space were: Young modulus $E = 210GPa$, Poisson's ratio $\nu = 0.3$. The hardening law for the elastic-plastic body was chosen as a power law (Swift's law):

$$\sigma_Y(e^p) = B(C + e^p)^n, \quad (17)$$

with $\sigma_Y(e^p)$ the yield strength function, e^p the effective accumulated plastic strain, and the following parameters: $B = 1280MPa$, $C = 30$, $n = 0.085$.

Normal residual displacement enters interference equation, by superimposing the deflections induced by pressure distribution. When only one of the contacting bodies, let it be body (2), is elastic-plastic and the other one, let it be body (1), is rigid or elastic, the following interference equation can be written:

$$h(i, j) = hi^{(1+2)}(i, j) + u_3^{pr(1+2)}(i, j) + u_3^{r(2)}(i, j) - \omega, \quad (18)$$

with h the gap in deformed state, hi the initial gap (or initial contact geometry), ω rigid body approach, u_3^{pr} the elastic part of displacement, namely that induced by contact pressure, and u_3^r the residual part of displacement, namely that induced by plastic region.

Profiles of residual prints corresponding to six loading levels are depicted in Fig. 1. These profiles show that residual displacement increase contact conformity in non-conforming contact, leading to a more uniform distribution of contact pressure. Therefore, pressure distribution in elastic-plastic contact appears flattened compared to the elastic case.

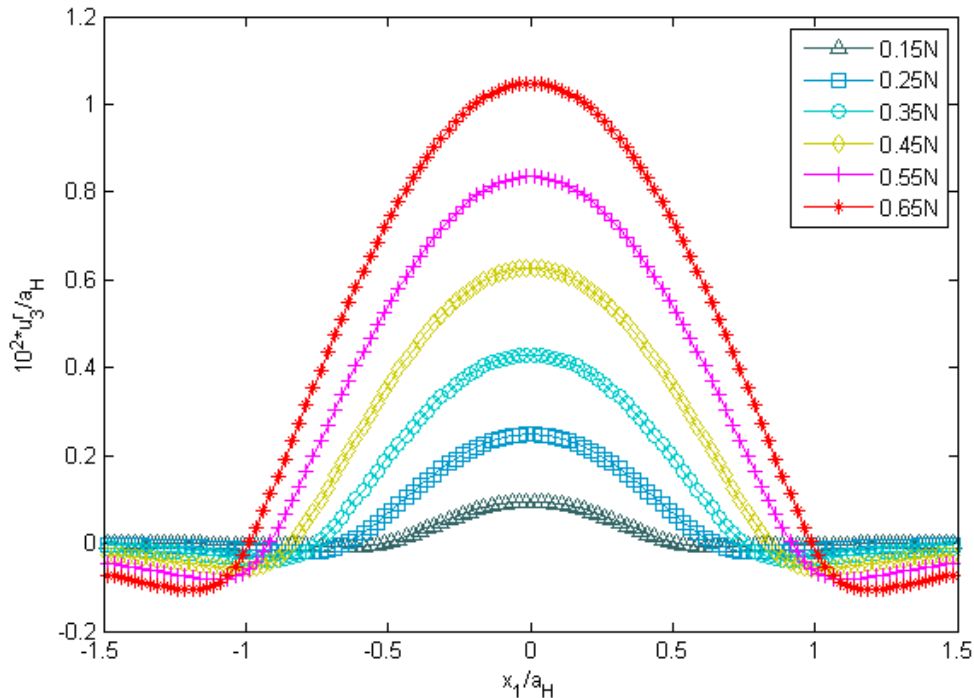


Figure 1. Residual print profiles in elastic-plastic spherical contact

The variation of residual print maximum depth with the loading level is presented in Fig. 2. This curve was also obtained experimentally by El Ghazal, [5], numerically by Jacq et al. [7], and also by Benchea and Cretu, [2], using finite element analysis.

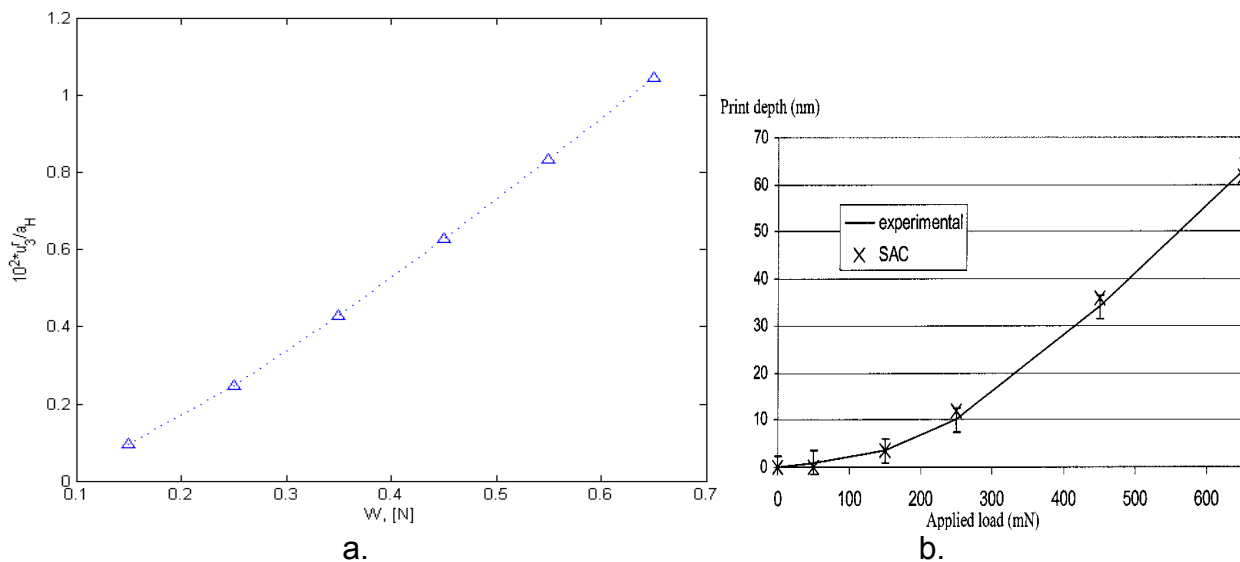


Fig. 2. Residual print depth: a. this code, b. Jacq et al. [7]

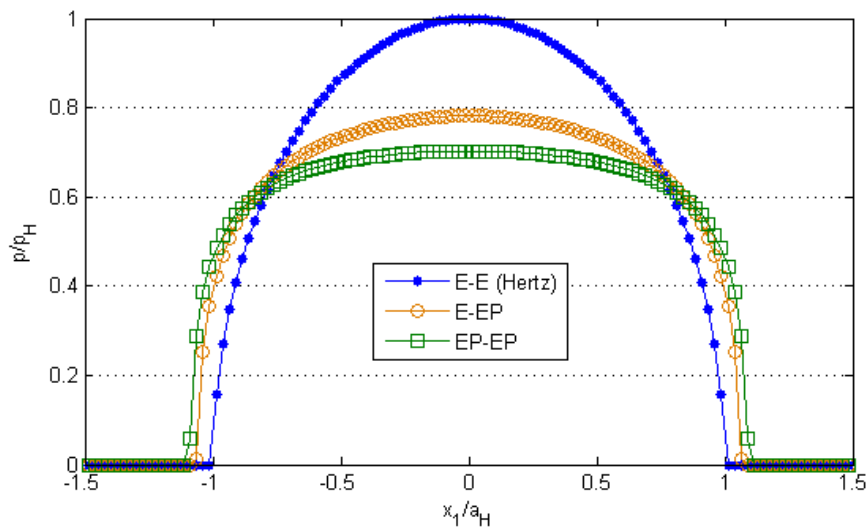
On the other hand, when contacting bodies are both elastic-plastic, eq. (18) encloses residual displacements of both surfaces:

$$h(i, j) = hi^{(1+2)}(i, j) + u_3^{pr(1+2)}(i, j) + u_3^{r(1+2)}(i, j) - \omega, \quad (19)$$

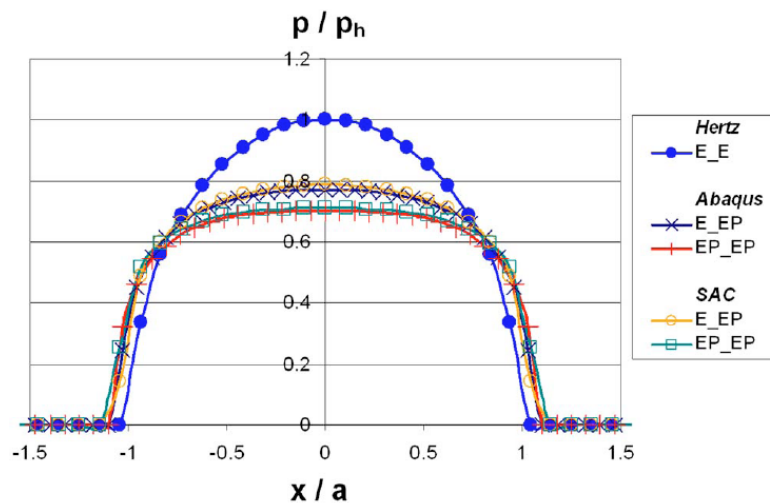
If the hardening behavior or contacting bodies is dissimilar, residual displacement should be computed for every body separately. The model is simplified considerably if the bodies follow the same hardening law and have the same contact geometry, because, due to symmetry of the problem about the common plane of contact, $u_3^{r(1)} = u_3^{r(2)}$. Consequently, eq. (19) becomes:

$$h(i, j) = hi^{(1+2)}(i, j) + u_3^{pr(1+2)}(i, j) + 2u_3^{r(2)}(i, j) - \omega. \quad (20)$$

To validate eq. 20, the contact between two spheres of radius $R = 0.015m$ is simulated numerically, for different material behaviors: purely elastic (E), and elastic-plastic (EP) following Swift's law, with the following parameters: $B = 945MPa$, $C = 20$, $n = 0.121$. The contact is loaded normally to a level of $W = 11179N$, corresponding to a hertzian pressure of $p_H = 8GPa$ and to a Hertz contact radius of $a_H = 817 \mu m$. Pressure distributions obtained using eq. (20), depicted in fig. 3a, agree well with already published results, fig. 3b.



a.



b.

Fig. 3. Pressure profiles for various material behaviors: a. this code, b. Boucly, Nélias, and Green [3]

4. EXPERIMENTAL VALIDATION

As contact mechanics uses simplifying assumptions in order to circumvent the mathematical complexity of the arising equations, experimental validation is needed to verify model viability. An extended program of experimental research was conducted in

the Contact Mechanics Laboratory of the University of Suceava, aiming to assess residual print parameters in rough elastic-plastic non-conforming contacts. The stand used was originally designed by Nestor et al. [12]. Microtopography of deformed surface was scanned with a laser profilometer UBM14. Some results, already published in [13], are used here to validate the numerical formulation.

Contact between a steel ball, assumed as a rigid indenter, and a lead specimen, simulating the elastic-plastic half-space, was simulated using the numerical formulation. As lead is best described as an elastic - perfectly plastic material, a linear hardening law with a very small slope was considered. Residual prints at two loading levels, corresponding to hertzian pressures of 0.48 GPa and of 0.94 GPa respectively, are depicted in figs 4 and 5.

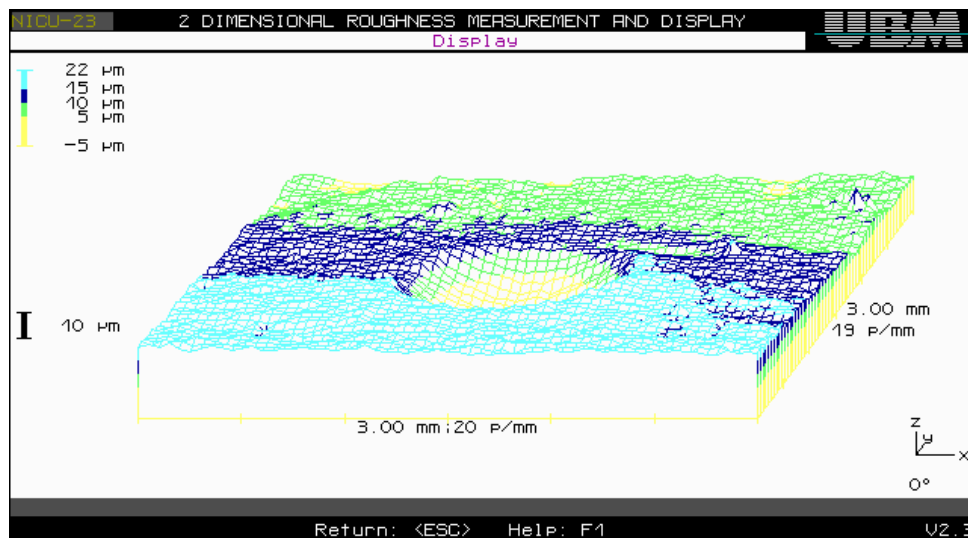


Fig. 4. Residual print, $p_H = 0.48 \text{ GPa}$, [13]

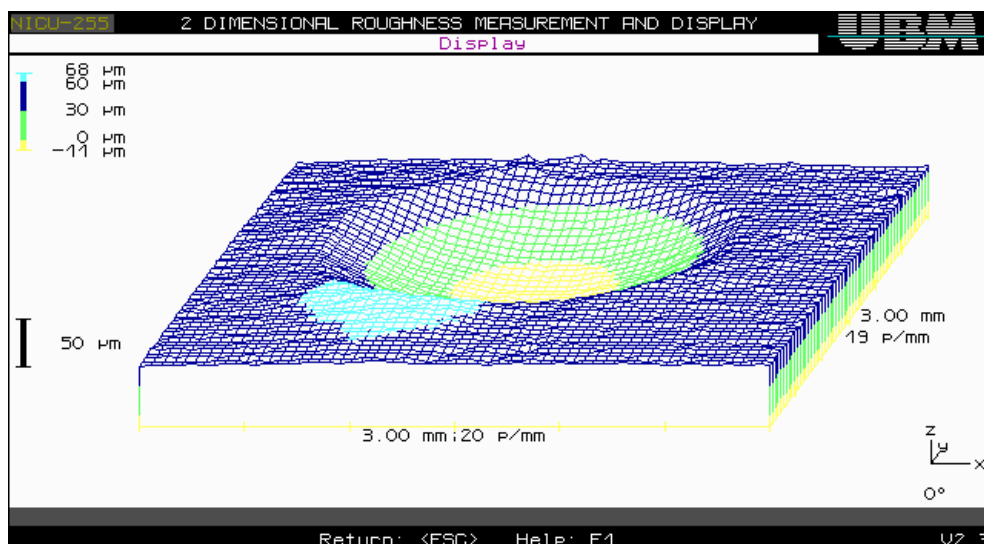


Fig. 5. Residual print, $p_H = 0.94 \text{ GPa}$, [13]

Variation of print depth with loading level is presented in fig. 6. The agreement between the values predicted by the numerical program and those obtained experimentally is satisfactory.

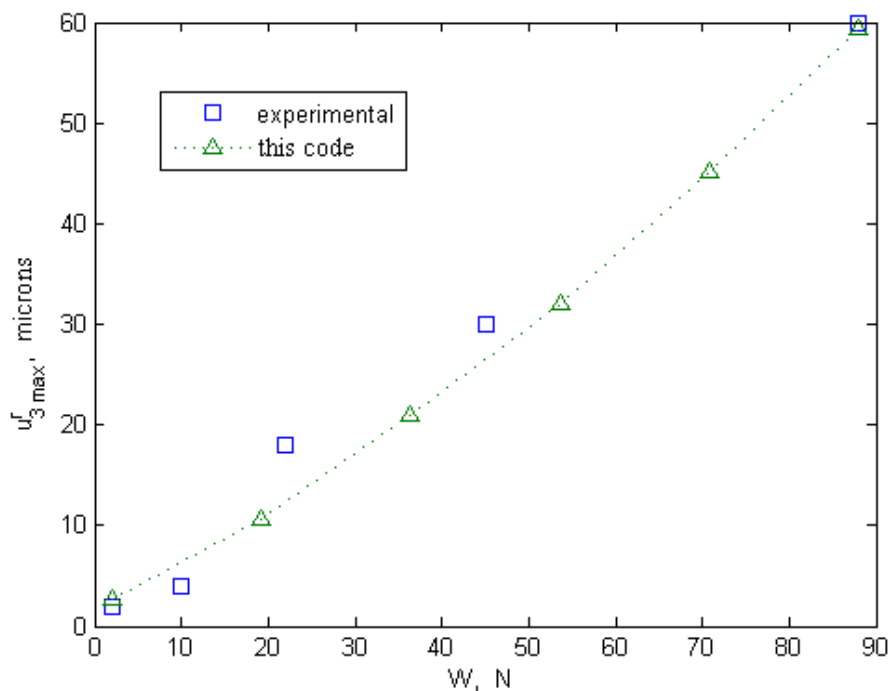


Fig. 6. Residual print depth versus loading level

5. CONCLUSIONS

Residual displacement is expressed in terms of plastic strains using Betti's reciprocal theorem. By imposing digitization of plastic strain region, residual print relation is formulated as a two-dimensional discrete cyclic convolution, computed by a two dimensional DCFIT algorithm. Formulas for influence coefficients are derived by integration of Boussinesq fundamental solutions over a cuboidal domain.

Three types of contacts, namely rigid – elastic-plastic, elastic – elastic-plastic and elastic-plastic – elastic-plastic, are simulated using the newly proposed code. The elastic-plastic behavior is described by a power hardening law (Swift). Numerical predictions agree well with already published results, obtained using alternative numerical codes or finite element analysis.

Numerical simulations predict that residual displacement increase contact conformity. Consequently, elastic-plastic pressure distributions appear flattened compared to elastic case, due to changes in both hardening state and contact conformity.

Residual print depths obtained experimentally from indentation of a lead specimen with a rigid sphere match well the numerical predictions, giving further confidence in the newly proposed program.

REFERENCES

- [1] Antaluca, E., (2005), *Contribution a l'étude des contacts élasto-plastiques - effet d'un chargement normal et tangentiel*, Ph.D. Thesis, INSA Lyon, France.
- [2] Benchea, M, and Crețu, S., (2008), *An Improved Incremental Model to Analyse Elastic - Plastic Concentrated Contacts – The Finite Element Analysis and Validation*, Acta Tribologica, Vol. 16, ISSN 1220-8434.
- [3] Boucly, V., Nélias, D., and Green, I., (2007), *Modeling of the Rolling and Sliding Contact Between Two Asperities*, ASME J. Tribol., **129**, pp. 235 - 245.
- [4] Boussinesq, J., (1969), *Application des potentiels à l'étude de l'équilibre et du mouvement des solides élastiques*, Reed. A. Blanchard, Paris.
- [5] El Ghazal, H., (1999), *Etude des propriétés microstructurales et mécaniques des aciers 16NiCrMo13 cémenté et 32CrMoV13 nitrure - Application a la prévision de leur limite d'endurance en fatigue de roulement*, Ph.D. Thesis, INSA Lyon, France.

- [6] Jacq, C., (2001), *Limite d'endurance et durée de vie en fatigue de roulement du 32CrMoV13 nitruré en présence d'indentations*, Ph.D. Thesis, INSA Lyon, France.
- [7] Jacq, C., Nelias, D., Lormand, G., and Girodin, D., 2002, *Development of a Three-Dimensional Semi-Analytical Elastic-Plastic Contact Code*, ASME J. Tribol., 124, pp. 653–667.
- [8] Liu, S. B., Wang, Q., and Liu, G., 2000, *A Versatile Method of Discrete Convolution and FFT (DC-FFT) for Contact Analyses*, Wear, 243 (1–2), pp. 101–111.
- [9] Liu, S. Wang, Q., 2005, *Elastic Fields due to Eigenstrains in a Half-Space*, ASME J. Appl. Mech. 72, pp. 871–878.
- [10] Mayeur, C., (1995), *Modélisation du contact rugueux élastoplastique*, Ph.D. Thesis, INSA Lyon, France.
- [11] Nélias, D., Antaluca, E., Boucly, V., and Crețu, S., (2007), *A Three-Dimensional Semianalytical Model for Elastic-Plastic Sliding Contacts*, ASME J. Tribol., 129, pp. 761 - 771.
- [12] Nestor, T., Prodan, D., Pătraș-Ciceu, S., Alaci, S., Pintilie, D., (1996), *Stand pentru determinarea histerezisului static la solicitarea de contact*, (in Romanian), Proceedings of VAREHD 8, Suceava.
- [13] Purice, B. N., (2005), *Cercetări experimentale prin profilometrie cu laser privind deformațiile plastice de contact*, (in Romanian), Graduation Thesis, Suceava.
- [14] Spinu, S., (2009), *Contributions to the Solution of the Elastic-Plastic Normal Contact Problem*, (in Romanian), PhD Thesis, University of Suceava, Romania.
- [15] Wang, F., and Keer, L. M., (2005), *Numerical Simulation for Three Dimensional Elastic-Plastic Contact With Hardening Behavior*, ASME J. Tribol., 127, pp. 494–502.